Direct observation of spin rotation in Bragg scattering due to the spin-orbit interaction in silicon

T.R. Gentile,[1] M.G. Huber,[1] D.D. Koetke,[2] M. Peshkin,[3,*] M. Arif,[4,*] T. Dombeck,[5,*]
D. S. Hussey,[1] D.L. Jacobson,[4] P. Nord,[2] D. A. Pushin,[6,7] and R. Smither[3]

[1]*National Institute of Standards and Technology, Gaithersburg, MD 20899, USA*
[2]*Valparaiso University, Valparaiso, IN 46383, USA*
[3]*Argonne National Laboratory, Argonne, IL 60439, USA*
[4]*Stop 8461, National Institute of Standards and Technology, Gaithersburg, MD 20899, USA*
[5]*University of Hawaii, Hilo, HI 96720, USA*
[6]*University of Waterloo, Waterloo, Ontario, Canada N2L 3G1*
[7]*Institute for Quantum Computing, Waterloo, Ontario, Canada N2L3G1*

(Dated: Sept. 11, 2019)

As a neutron scatters from a target nucleus, there is a small but measurable effect caused by the interaction of the neutron's magnetic dipole moment with that of the partially screened electric field of the nucleus. This spin-orbit interaction is typically referred to as Schwinger scattering and induces a small rotation of the neutron's spin on the order of 10^{-4} rad for Bragg diffraction from silicon. In our experiment, neutrons undergo greater than 100 successive Bragg reflections from the walls of a slotted, perfect-silicon crystal to amplify the total spin rotation. A magnetic field is employed to insure constructive addition as the neutron undergoes this series of reflections. The strength of the spin-orbit interaction, which is directly proportional to the electric field, was determined by measuring the rotation of the neutron's spin-polarization vector. Our measurements show good agreement with the expected variation of this rotation with the applied magnetic field, while the magnitude of the rotation is ≈40 % larger than expected.

I. INTRODUCTION

The neutron spin-orbit interaction, or Schwinger scattering, which results from the interaction of a moving neutron's magnetic dipole moment (MDM) with the atomic electric field, induces a small rotation of the neutron's spin orientation in one Bragg reflection [1]. This effect was first studied in the scattering of fast neutrons from heavy nuclei [2–7]. For slow neutrons, the spin-orbit interaction was first determined in vanadium by measuring its spin-dependent scattering [8]. Vanadium was employed because its small coherent scattering length made the measurement possible. In that work, measurements were also performed on silicon and NaCl, but the data were consistent with zero within uncertainties due to the larger coherent scattering lengths of those samples. Spin-polarization-sensitive scattering was observed in the scattering of neutrons by CdS [9]. In a later experiment performed in the Laue geometry and employing neutron spin-Pendellösung resonance, a 17.8 % larger effect than expected from theory was observed in silicon, whereas the experimental uncertainty was 1.8 % [10].

The interaction of neutrons with the strong atomic electric field during Bragg reflection was exploited to search for a neutron electric dipole moment (EDM) [11], but this approach has been superseded by nuclear magnetic resonance methods with ultracold neutrons [12, 13]. The Schwinger interaction of polarized neutrons with the electric field of a noncentrosymmetric perfect crystal has been investigated for neutron EDM searches [14, 15].

Here we report a measurement of the neutron spin-orbit interaction in silicon using the technique of multiple Bragg reflections to increase the strength of the observed spin-orbit signal. The experiment was carried out on the NG-6A beam line at the NIST Center for Neutron Research (NCNR), where NG denotes neutron guide. In principle, the power of the Bragg reflection method could be greatly increased by the use of multiple reflections because the sensitivity to a neutron EDM is directly proportional to the number of successive Bragg reflections. The work described here is the first test of this method using multiple Bragg reflections from a silicon crystal.

II. THEORY

When a neutron moving with velocity $\vec{v}$ scatters from a silicon atom it will move through the electric field $\vec{E}$ that is due to the nuclear charge modified by the atomic electron screening. In the neutron rest frame this motion induces an effective magnetic field

$$\vec{B}_{\text{eff}} = \frac{1}{c}\vec{v} \times \vec{E} \tag{1}$$

where c is the speed of light. (Following prior literature, we employ Gaussian units for this discussion.) In this induced magnetic field a neutron with spin-polarization $\vec{P}$ will experience a torque on its magnetic dipole moment, $\vec{\mu}_{\text{n}} = \mu_{\text{n}}\vec{P}$, that is

$$\vec{\tau}_{\text{MDM}} = \mu_{\text{n}}\vec{P} \times \vec{B}_{\text{eff}} \tag{2}$$

*deceased

This torque will rotate the polarization orientation around $\vec{B}_{\rm eff}$. This effective magnetic field gives rise to the spin-orbit interaction energy, V, that was first described quantitatively by Schwinger [1] and employed in Ref. [8]:

$$V = \frac{\mu_{\rm n}}{mc}\vec{P}\cdot(\vec{p}\times\vec{E}) \tag{3}$$

Here $\vec{p} = m\vec{v}$ is the neutron momentum and m is the neutron mass. Thus, the neutron scattering length $b_{\rm r}$ will consist of two terms

$$b_{\rm r} = b_{\rm c} \pm i|b_{\rm so}|. \tag{4}$$

$b_{\rm c}$ is the spin-independent coherent nuclear scattering length for silicon, $b_{\rm so}$ is the spin-orbit (Schwinger) scattering length, given by

$$b_{\rm so} = \frac{\mu_{\rm n}}{\hbar c}Ze(1 - f_{220})\cot\theta_{\rm B}. \tag{5}$$

and the sign depends on the neutron polarization direction. Here $\theta_{\rm B}$ is the Bragg angle, Ze is the nuclear charge, and f_{220} is the form factor for the charge distribution of the atomic electrons for the (220) Bragg reflection [16].

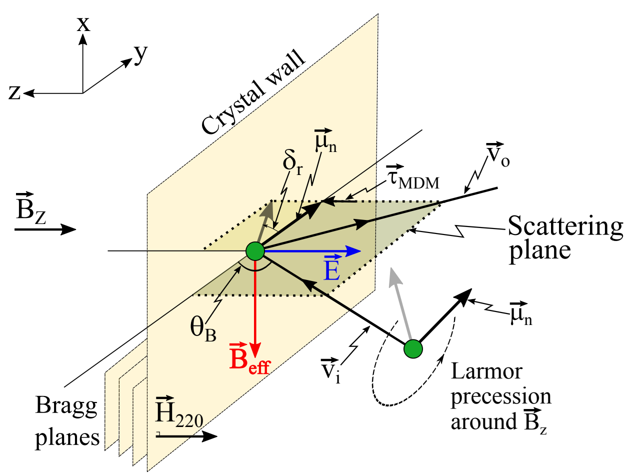

FIG. 1: Shown is the orientation and coordinate system for a neutron with magnetic dipole moment $\vec{\mu}_{\rm n}$ scattering from the (220) Bragg planes of a perfect silicon crystal. The electric field $\vec{E}$ (blue) of the silicon atoms combined with incident neutron velocity $\vec{v}_i$ induces an effective magnetic field $\vec{B}_{\rm eff}$ (red). When $\vec{\mu}_{\rm n}$ is aligned to the y-axis, a torque $\vec{\tau}_{\rm MDM}$ in the z-direction rotates the MDM through a maximum angle $\delta_{\rm r}$. Outside of the crystal, $\vec{\mu}_{\rm n}$ precesses around the applied external field $\vec{B}_z$.

The neutron scattering plane, as depicted in Fig. 1, is defined by the cross product $\vec{v}_o \times \vec{v}_i = nv^2\sin(2\theta_{\rm B})$ where n is the index of refraction and $\vec{v}_i$ and $\vec{v}_o$ are the incident and outgoing neutron velocity vectors, respectively. (Because the recoil energy of the silicon atom bound in the crystal is negligible the process is elastic and $|\vec{v}_i| \approx |\vec{v}_o|$). The electric field $\vec{E}$ is directed along the momentum transfer vector, normal to the crystal planes [16]. We align the incident neutron beam to be in the horizontal y-z plane so that, in the absence of divergence, $\vec{v}_i$ and $\vec{v}_o$ will each have only v_y and v_z components. The v_z components (incoming and outgoing) are parallel to $\vec{E}$ so it is only the v_y component that will contribute to $\vec{B}_{\rm eff}$ in Eq. (1).

Taking the Bragg angle $\theta_{\rm B}$ in Eq. (5) to be 85°, $\mu_n = -1.91$ nuclear magnetons, where the nuclear magneton is 5.05×10^{-24} erg/G, $e = 4.803\times10^{-10}$ statcoul, $Z(1-f_{220}) = 5.612$ [17], $m = 1.67\times10^{-24}$ g, and $c = 3.00\times10^{10}$ cm/s we obtain $b_{\rm so} = 7.22\times10^{-17}$ cm. Using neutron interferometry $b_{\rm c}$ has been measured to high precision to be 0.415×10^{-12} cm [18].

Because $b_{\rm so} \ll b_{\rm c}$ we can approximate the scattering length as

$$b_{\rm r} \approx b_{\rm c}\exp\left[i\beta(\pm P_z)\right] \tag{6}$$

where P_z is the neutron spin component along the z-axis and

$$\beta(\pm P_z) \approx |b_{\rm so}/b_{\rm c}| \tag{7}$$

represents the spin dependent phase angle induced by the spin-orbit interaction coupling to the neutron MDM. Thus, if the neutron spin is in the x-y plane (aside from the special case of the spin along the x-axis) it will experience a rotation about $\vec{B}_{\rm eff}$ that will rotate it out of the x-y plane giving it a z-component. The expected magnitude of this rotation angle can be estimated as

$$\delta_{\rm r} = 2|b_{\rm so}/b_{\rm c}| \tag{8}$$

which for the values above gives 3.27×10^{-4} rad.

Moreover, while the neutron wave reflects off multiple atomic planes, for large Bragg angles, $\lambda_{\rm B} \approx 2d_{220}$, where $\lambda_{\rm B}$ is the Bragg-diffracted neutron wavelength and d_{220} is the lattice spacing for the (220) plane. Each successive plane contributes an unimportant phase shift $\Phi = n2\pi$ (where n is an integer) to the overall scattered wave plus the spin-orbit phase shift generated at the atomic sites where the wave scatters. Therefore, when scattering occurs in a perfect silicon crystal each part of the induced neutron wave front reflected from successive crystal planes contributes coherently to the reflected wave.

The scattering induced z-component of the neutron spin polarization P_z is evidence of the spin-orbit interaction. However, because of the exceptionally small size of this effect on a single scatter it has presented experimental challenges in past attempts to measure this effect in silicon [8].

It is evident that when the spin orientation $\vec{P}$ is parallel to the y-axis when reaching the crystal surface that the rotation about $\vec{B}_{\rm eff}$ will produce the largest z-component P_z. If the polarization is aligned with the x-axis upon reaching the crystal surface there will be zero rotation as $\vec{P}$ is parallel to $\vec{B}_{\rm eff}$. Between these two extremes, the P_z induced will be proportional to $\cos(\phi)$ where ϕ is the angle between $\vec{P}$ and the y-axis at the crystal surface. (For example, if $\phi = \pi$ the rotation will induce a component of the spin polarization in the opposite z direction.) Therefore, for completeness we write the size of the induced Schwinger spin-orbit rotation on one reflection as $\delta_{\rm so} = \cos(\phi) \times 3.27 \times 10^{-4}$ rad.

To amplify the signal size from a single reflection we have devised a method to have multiple sequential Bragg reflections in a single crystal by cutting a slot in the crystal parallel to the (220) planes wherein the neutrons will sequentially reflect off opposing walls of the slot. These sequential reflections will occur at identical Bragg angles and according to neutron diffraction theory [3] those neutrons with wave vectors k that fall within the narrow range $k_{\rm P} - k_{\rm D} < k_z < k_{\rm P} + k_{\rm D}$ will be almost 100 % reflected. Here k_z is the z-component of the neutron wave number, $k_{\rm P}$ is the value of k_z at the center of the scattering peak and $k_{\rm D}$ is half the Darwin width, which is approximately $10^{-4}k_{\rm P}$. Neutrons within the Darwin width will be nearly 100 % reflected on subsequent encounters with the walls of the crystal slot as they progress in the y-direction down the slot. The reflectivity for neutrons outside the Darwin width drops rapidly as a function of k_z so these neutrons will be lost after a few reflections.

To see how multiple Bragg reflections of the neutron in the silicon slot with parallel walls can amplify the Schwinger signal, consider the first reflection to have $\vec{P}$ incident along the y-axis. The spin-orbit interaction will rotate $\vec{P}$ through an angle $\delta_{\rm so}$ thereby inducing a z-component P_z. (See Fig. 1.) After the first reflection, the neutron will reach the second reflection along the opposite wall in the slot where the electric field points opposite to the first reflection, i.e, $\vec{E} \to -\vec{E}$. As a result, the induced $\vec{B}_{\rm eff}$ and the associated torque will be opposite to that on the first reflection. Thus, the second reflection will cause $\vec{P}$ to rotate opposite to that on the first reflection and the net P_z after two reflections will be zero. To rectify this problem and make the multiple Bragg reflections all additive we placed the crystal in a uniform magnetic field parallel to the z-axis, B_z, so that the neutron polarization will precess about B_z as the neutron crosses the slot. If we set the magnitude of B_z to cause $\vec{P}$ to precess through an angle of π radians then on subsequent reflections the $\vec{E}$-field, $\vec{B}_{\rm eff}$, and the polarization $\vec{P}$ will all change sign so that the torque on the neutron MDM will be consistently in the same direction on each reflection. Thus the incremental changes in P_z will all be in the same direction and will, therefore, be additive. For example if the crystal slot is 10 mm wide and 120 mm long we expect to have 136 reflections for a Bragg angle of 85° which, in turn, will yield $136\delta_{\rm so} = 136\cos(\phi) \times 3.27 \times 10^{-4}$ rad= 0.0473 rad (for $\phi = 0$), which is measureable. We were, in fact, able to measure the change in the resultant magnitude of P_z due to the $\cos(\phi)$ dependence explicitly (see Sec. IV B).

The final magnitude of the Schwinger signal $P_z^{\rm tot}$ after transiting a slot with length/width ratio of L/d_z is surprisingly independent of $\theta_{\rm B}$. From Eq. (5) we see that the spin-orbit scattering length for one reflection is proportional to $\cot(\theta_{\rm B})$ which implies that the Schwinger signal after one reflection is also proportional to $\cot(\theta_{\rm B})$. However, for a slotted crystal the total number of reflections is

$$N^{\rm tot}(\theta_{\rm B}) = (L/d_z)\frac{1}{\cot\theta_{\rm B}}. \quad (9)$$

Therefore, the dependence of $P_z^{\rm tot}$ on $\theta_{\rm B}$ is perfectly cancelled by the product of the signal ($\propto \cot(\theta_{\rm B})$) with the number of reflections ($\propto 1/\cot(\theta_{\rm B})$). The only experimental parameter to increase or decrease the Schwinger signal using this technique is by using a crystal with a different L/d_z ratio.

III. METHOD AND APPARATUS

A. Overview

We show in Fig. 2 a diagrammatic layout of the apparatus and in Figs. 3 and 4 photographs of the apparatus as installed at a Bragg angle $\theta_{\rm B} = 85°$. The neutrons enter the slot of the silicon crystal where they Bragg scatter off opposing walls thereby amplifying the incremental spin-orbit rotation of the polarization vector. This results in a definitive z-component, $P_z^{\rm tot}$, when leaving the crystal slot that is measured using a polarization analyzer. Details of the method and the apparatus are described in the following sections.

B. Silicon crystal

The slotted crystal was commercially fabricated from a float-zone grown, perfect silicon crystal. The crystal was 5.5 cm high x 3.0 cm wide x 14.0 cm long with a 1.0 cm wide x 4.0 cm deep slot machined down the center along the long axis of the crystal (see Fig. 4) leaving 1.0 cm thick walls. In addition, 1.0 cm of the upstream (downstream) wall was removed to allow the neutrons to enter (leave), hence the slot length for multiple Bragg reflections was 12.0 cm.

Subsequent to machining and etching the crystal was received at NIST where measurements of the slot width showed a substantial variation along the length of the crystal (y-axis) and along the vertical (x-axis) as seen in Fig. 5. A computer simulation of the neutron trajectories down the fabricated slot for the 136 Bragg reflections obtained at $\theta_{\rm B} = 85°$ showed that the resultant spin-orbit induced rotation of the polarization vector $P_z^{\rm tot}$ would be

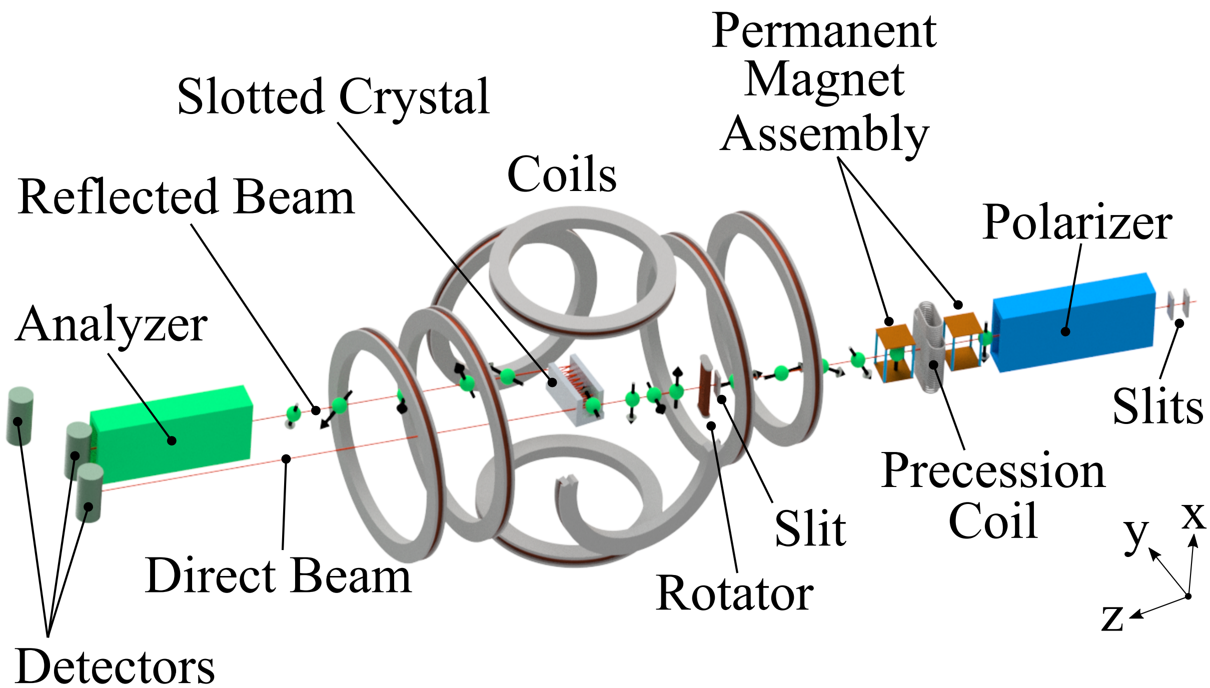

FIG. 2: Layout of the apparatus for the study of the neutron spin-orbit interaction. The neutron beam travels from right to left. The monochromatic neutron beam passes through a supermirror polarizer (enclosed in blue steel yoke), a vertical guide field, precession coil π-flipper, another vertical guide field, and into the magnetic field region generated by the four axial coils. At the center of this region (see Fig. 4) the beam passes through a collimator and a spin rotator, and is incident on the slotted crystal. Most of the neutrons (denoted "direct beam") pass through the crystal wall, whereas the small fraction within the Darwin width is reflected (denoted "reflected beam") and undergoes 136 reflections before exiting the slot. The supermirror analyzer (enclosed in green steel yoke) can be translated to analyze the neutron polarization in either the reflected beam or the direct beam. Each of these beams is detected by a ^{3}He neutron detector.

≈ 75 % of what was expected from a crystal with parallel walls.

C. Magnetic field

As mentioned in Sec. II, the crystal was placed in a uniform magnetic field along the z-axis, perpendicular to the (220) crystal planes (see Fig. 1). The magnetic field was required to be uniform to a few parts per thousand over the volume of the crystal and with no unwanted transverse fields. The z-axis field, B_z, was obtained using two pairs of coils with spacings and relative currents that were determined by computer modeling. To cancel any transverse fields, coil pairs were employed along the x and y axes. The design magnitude of the B_z field was approximately 1.8 mT (18 G). All eight coils were mounted on a rigid aluminum frame. The coils are shown in Fig. 2 and the photograph in Fig. 3.

To measure field uniformity, a calibrated triple axis Hall probe mounted on a long non-magnetic arm was positioned at multiple points on a 3-D grid inside the coil system using a programmable three-axis translation stage. The magnetic field readings were taken at various predetermined currents in the four axial coils. The measured B_z values were consistent with the calculations and the field uniformity was within the established tolerances. Using a flux gate magnetometer that was mounted on the eight-coil magnet frame, we observed that the magnetic field remained constant within our established tolerances.

The absolute magnetic field as a function of the currents in the coils at the crystal slot was determined to an accuracy of order 0.01 % using a free induction decay (FID) nuclear magnetic resonance [19] signal from a cell of polarized ^{3}He gas. The 5 cm diameter, 5 cm long cell was placed in the location where the slotted crystal normally resides. By translating the cell along the y-axis and observing the frequency of the FID signal we

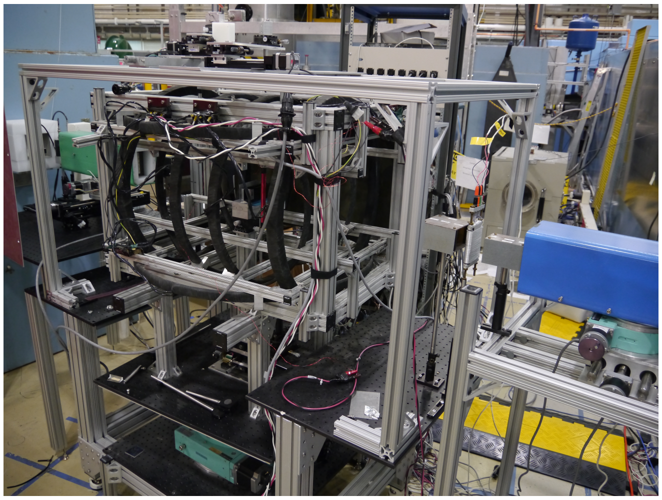

FIG. 3: Photograph of the apparatus for study of the neutron spin-orbit interaction. The beam travels from right to left.

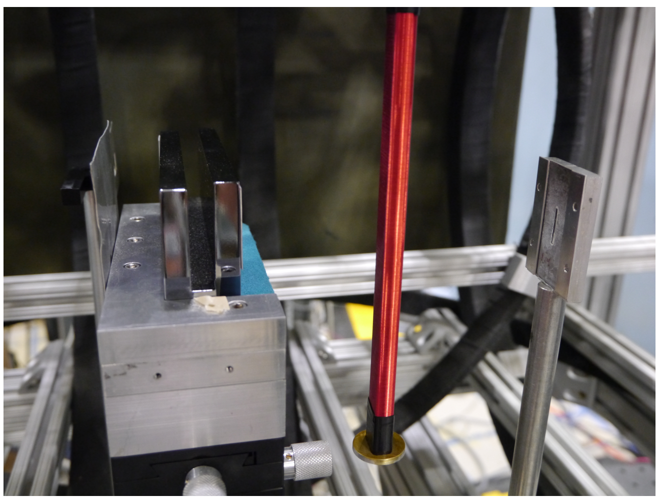

FIG. 4: Photograph showing the collimator, rotator coil. and crystal. The beam travels from right to left. Cadmium located just downstream of the crystal blocked neutrons scattered during passage along the slotted crystal.

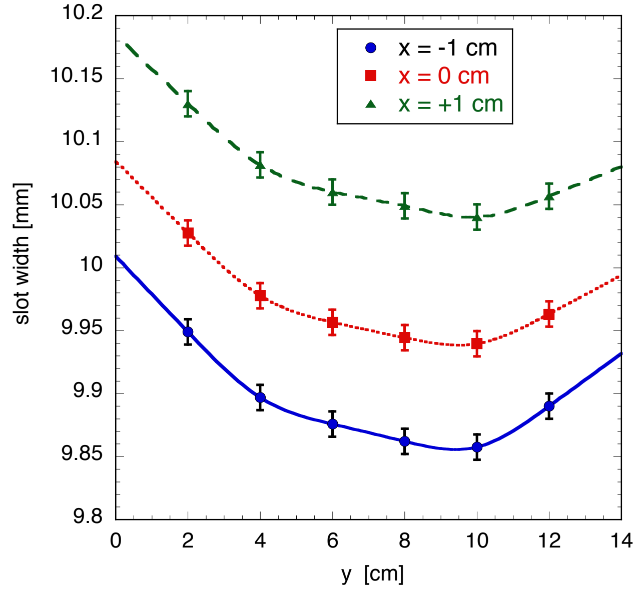

FIG. 5: Spatial variation of the slot width. The points show measurements of the slot width and the lines show spline fits that were employed for calculating the expected spin rotation. The beam height is limited to the range -0.5 cm $\leq x \leq 0.5$ cm by a 1 cm tall collimator located at the end of the crystal. The error bars indicate the uncertainty from the coordinate measuring apparatus employed.

determined that the variation in the magnetic field was only ≈0.03 % over the length of the slot. For a uniform slot with a width of 9.952 mm, the maximum Schwinger rotation is expected at a magnetic field B_z^0=1.7672 mT (17.672 G).

D. Alignment

The origin of the xyz coordinate system previously defined was taken to be at the vertical (x) and horizontal (y) center of the crystal slot and with z=0 at the surface of the downstream wall of the slot. The x-axis points upward out of the crystal slot and the y-axis is along the slot in the direction of the neutron travel down the slot. The initial alignments were done using a theodolite and a laser system. Later, these alignments were fine-tuned using neutrons in our direct beam. The aluminum frame for the magnetic field coils was supported by a y-z translation stage, a 2D (y and z) tilt stage, and a stage that provided rotation about the x-axis; the last of which permitted the coils and crystal to be co-rotated. The collimators, the upstream supermirror polarizer, the permanent magnet guide fields, the rotator coil, the supermirror analyzer detector, and the ^{3}He detector were aligned for the direct neutron beam to properly pass through each. The location of the analyzer in the direct beam was permanently referenced so it could easily and accurately be translated on a screw-driven stage between this position and its location in the outgoing reflected beam. The axis of the four-coil magnet system was aligned to be parallel to the incoming neutron beam. The position of the crystal was aligned so that the x-y center of the crystal slot is located at the x-y-z center of the four-coil magnet system.

With the crystal slot oriented perpendicular to the incoming beam the entire assembly was translated so the incoming beam passed as close as possible to the upstream wall of the crystal to strike the downstream wall. Therefore, the neutron beam transits into (and leaves from) the four-coil field region along trajectories that are displaced from the magnet center by half the crystal slot length. In this orientation adjustments were made so that the axis of rotation of the entire assembly was parallel to the x-axis and centered at the point where the neutron beam strikes the downstream slot wall for the first reflection. All these alignments were then fixed so that going forward there was no further motion of the crystal relative to the four-coil magnet system. The crystal and the four-coil magnet system (fixed together) were rotated to the intended Bragg angle θ_{B} relative to the incoming beam direction. This preserved the magnetic field B_z direction to be perpendicular to the (220) planes. The collimator and the vertical rotator coil seen in Fig. 4 remained aligned in the direct beam. Finally, the spin-analyzer and a ^{3}He filled neutron detector were aligned with the reflected neutron beam that leaves the crystal slot.

E. Neutron transport

1. *To the slotted crystal*

The NG-6 neutron beam was reflected by a 30 mm x 30 mm x 10 mm pressed silicon (111) polycrystalline monochromator to produce a monochromatic neutron beam with a wavelength distribution that was centered at 0.3833 nm and had a full width at half maximum (FWHM) of 0.0017 nm. Because the (222) reflection is forbidden, there is no component at half this wavelength in the beam. Vertical and horizontal collimators 6 mm x 6 mm were located upstream of the polarizer and a slit 1.4 mm wide and 13 mm tall was positioned 15 cm upstream of the first reflection off the silicon crystal. As discussed in Sec. II, only neutrons within the narrow Darwin width are reflected; for $\theta_{\mathrm{B}} = 85^\circ$, the wavelength selected is 0.3825 nm which is well within the FWHM provided by the monochromator.

A supermirror [20] polarized the neutron spin to be parallel to the x-axis and was positioned just after the upstream collimators. A guide field aligned with the polarizer field, made using two permanent magnets, was positioned between the x-axis polarizer field and the z-axis field of the four-coil system. Between the two permanent magnet assemblies was a precession coil π-flipper [20] consisting of two aluminum windings that provided fields in the vertical (cancellation) and transverse horizontal (precession) directions; the current in the cancellation coil was adjusted to cancel the guide field and the current in the precession coil was adjusted to rotate the neutron spin using Larmor precession. The precession coil π-flipper was used to measure the flipping ratio [20], which is defined as the ratio of the count rate detected by a spin-polarization analyzer for the polarization directly from the polarizer (flipper off) to the count rate with the polarization reversed (flipper on). A larger flipping ratio implies better alignment and higher efficiencies of the polarizer and the analyzer as well as other components affecting the spin transport. A flipping ratio of 23 was measured in the direct beam and is primarily due to the polarizing efficiencies of the polarizer (P_{p}) and analyzer (A_{a}) supermirrors of ≈ 0.96. In a similar exercise we measured a flipping ratio of 15 for neutrons reflected down the crystal slot. This small reduction (note that the product $P_{\mathrm{p}}A_{\mathrm{a}}$ only decreases from 0.917 to 0.875) may be due to a larger beam at the analyzer due to divergence of the beam in the 136 cm of additional travel due to the 136 reflections in the slot. Aside from these initial alignments and some systematic tests, the precession coil π-flipper was not energized during typical Schwinger measurements.

Neutrons that emerged from the upstream permanent magnet guide fields where the polarization was in the x-direction transition into the fringe field of the four-coil system where their dipole moments were adiabatically rotated [20] to be along the B_z-direction. The degree to which the neutron spin follows the magnetic field is related to the ratio of the Larmor frequency to the rate of change of the magnetic field vector experienced by the neutron. The neutrons continued toward the crystal until they encountered the vertical rotator coil immediately after the collimator. The rotator coil was used to rotate the neutron spin from parallel the z-axis to parallel with the x-axis upon leaving the coil. The rotator was designed to be 20 cm vertically long such that its return field had a negligible effect on the overall magnetic field gradient. The frame on which the coils were wound had a rectangular hole in it to allow the neutrons to pass through. The neutrons did pass through the copper wire windings. The rotator coil was mounted from above, independent of the eight-coil magnet frame. The rotator could be translated along the direction of the direct beam that so that the orientation of the neutron polarization on the first reflection at the crystal could be varied.

The rotator was designed to produce a field $\vec{B}_{\mathrm{r}}$ parallel to the x-axis with a magnitude equal to B_z. The addition of these two fields would result in a magnetic field, $\vec{B}_{\mathrm{net}}$, that was oriented at 45° with respect to the z-axis in the x-z plane and had a magnitude of $\sqrt{2}B_z$. The distance across the coil was chosen so that the transiting neutrons will Larmor precess by π rad around the resulting field in the coil thereby rotating the polarization of the neutron from the z-axis to the x-axis. Upon leaving the rotator coil the neutrons precessed in the x-y plane perpendicular to the B_z axis. In practice, once the coil dimensions are fixed, this will work in this manner for only one neutron wavelength (velocity) and for one B_z. With this in mind the rotator was fabricated so the distance across the rotator was close to what was expected for the intended neutron wavelength (velocity) and for the expected B_z. Then, to achieve the desired change in the neutron polarization the current in the rotator coil was adjusted to produce a flipping ratio of unity, which occurs when the neutron spin is transverse to the z-axis as intended. This exercise was performed at two different values of B_z: B_z^0=1.7672 mT (17.672 G) and 1.710 mT (17.10 G). Although the rotator current would be expected to be directly proportional to B_z, we found that the ideal currents for these two field values differed by 5.0 % (rather than 3.6 %) We determined the desired currents for other magnetic field values based on these measurements. Any small error in the rotation of the neutron spin will only produce a small component of the polarization, P_z, to which the spin-orbit induced values of P_z will be added. The orientation of the neutron polarization at the first reflection on the crystal was determined by the angle through which the neutron polarization rotates in the x-y plane after leaving the rotator coil. This angle depends on the Larmor precession frequency, the neutron velocity, and the distance from the rotator coil to the crystal.

Setting the four-coil magnetic field to the desired value for the Schwinger scattering measurement (described below) and knowing the neutron wavelength and velocity we calculated the Larmor precession period and the distance, $\Lambda = 20.0$ mm, that the neutron would travel in one Larmor period. Separately, we also measured this distance Λ in the direct beam by translating a second rotator coil with the same current as the first rotator coil and found it to agree with the calculated value Λ within 0.2 %.

As noted in Sec. II, the maximum Schwinger rotation will be induced when the spin polarization at the time of the first reflection from the crystal wall is parallel to the y-axis. Therefore, the rotator coil was positioned so that the distance from the exit of the coil to the first reflection, D_r, was 55 mm from the first reflection, i.e., 2.75 Λ corresponding to a spin precession of $2.75 \times 2\pi$. (The choice of 55 mm was in part dictated by the range of motion of the rotator coil.)

2. *Reflected down the crystal slot*

To fully understand the response from the neutron multiple Bragg scatters down the crystal slot we systematically changed the polarization orientation in the x-y plane at the first reflection. This was accomplished by varying the distance D_r from the rotator coil to the crystal face over a distance of 21 mm, slightly more than Λ=20.0 mm. It was expected that a plot of P_z^tot vs D_r would be sinusoidal.

In addition, the measurements described in the preceding paragraph were repeated with different values of B_z. Our simulations predicted that the resulting P_z^tot should be very sensitive to the magnitude B_z because when the B_z is not at its optimum value to produce the required π precession of the polarization vector when crossing the crystal slot the resulting size of the spin-orbit interaction on succeeding reflections will become progressively weaker as the orientation of the polarization vector at encounters with the walls drifts further away from the y-axis. Details of these measurements are described in section IV.

3. *From the crystal to the analyzer*

Following the last Bragg reflection at the end of the crystal slot the spin of the neutrons continued to precess around B_z. The polarization now had two components: a large component transverse to B_z (in the x-y plane) and a smaller component P_z^tot along the z-axis. The rotating polarization vector $\vec{P}$ traced out a cone with a large opening angle.

As the neutrons transitioned from the four-coil magnetic field to the vertical (x-direction) fringe field of the supermirror spin-analyzer magnet, seen in Fig. 2, their spin was adiabatically rotated so that P_z^tot would align with the vertical field. In the absence of a Schwinger interaction, the neutron spin would be precessing around this vertical axis, yielding half the count rate as compared to if the neutron's spin were aligned with this axis of the analyzer. The Schwinger signal P_z^tot thus modulated this otherwise constant count rate.

4. *Neutron detection*

Neutrons were detected using 12.7 mm diameter, ^{3}He proportional counters which have nearly 100 % detection efficiency. Each detector was encased in boron carbide shielding with a small opening to accept the neutrons from the intended source while limiting the solid angle available for background neutrons to be counted. Three ^{3}He detectors were used: one for measurement of neutrons exiting the slot, one to monitor changes in background rates, and lastly one to measure the direct beam rate. All data collected in the reflected beam were normalized to the corresponding direct beam counts to correct for any variations in the incident neutron flux. A fission chamber located just downstream of the pressed silicon monochromator was used to monitor reactor fluctuations.

To continuously monitor for any changes in ambient neutron background due to neighboring apparatus, a partially shielded ^{3}He background detector was located near the reflected beam detector. The actual background in the reflected beam detector was determined by registering the count rate in the reflected beam detector when the beam shutter was open and the crystal was rotated to $\theta_\mathrm{B} = 90°$ so that no neutrons were reflected down the slot but could scatter off of the silicon bulk. The background was found to be nearly constant as a function of time.

F. Computer simulation of Schwinger scattering in the slotted crystal

In a perfect slotted crystal with parallel walls separated by 10 mm we expect to have a Schwinger spin-orbit rotation of the neutron MDM vector of $\delta_\mathrm{so} = 3.27 \times 10^{-4}$ rad on each neutron Bragg reflection and total rotation of

$N_R\delta_{so} = 0.0473$ rad after $N_R = 136$ consecutive identical Bragg scatters. This assumes that the neutron MDM vector is properly aligned with the y-axis on the first reflection and B_z is set to produce a π-rotation on each crossing so that for all reflections the MDM vector is aligned with the y-axis producing the maximum Schwinger rotation. If, however, the crystal walls are not perfectly parallel such that the distance across the slot varies and/or B_z is not set to produce a π-rotation on each crossing then the MDM vector on reflection will not be aligned with the y-axis. The effect of this is to reduce the magnitude of the total Schwinger spin-orbit rotation by a factor $\cos(\phi)$ where ϕ is the angle between the MDM vector and the y-axis, i.e. $\delta_{so}\cos(\phi)$.

As seen in Fig. 5, the walls of our crystal are not properly parallel. To estimate the expected $\delta_{so}\cos(\phi)$ for each reflection for this crystal we wrote a computer simulation that took as input splines of the measured distance across the crystal slot as a function of location along the slot. The neutron beam vertical acceptance in the crystal was 1 cm that was centered vertically in the crystal slot. The simulation followed 11 horizontal neutron trajectories separated vertically by 1 mm down the crystal slot reflecting off opposing walls, for which the separation was determined from the measured distance across the slot at each reflection position $y(i)$. The small vertical beam divergence (defined by the 6 mm aperture located 170 cm upstream of the crystal and the 10 mm aperture just downstream of the crystal) was neglected. The distance $d_y(i)$ traveled in the y-direction during slot crossing i can be written as

$$d_{y(i)} = v_z \cot(\theta_B) * t_{slot}(i) \tag{10}$$

where

$$t_{slot}(i) = \frac{d_z(i)}{v_z}. \tag{11}$$

$d_z(i)$ is the distance across the slot at that y-location and t_{slot} is the time it takes the neutron to cross the slot. The distance across the slot for a given trajectory is found by interpolation from the measured slot widths shown in Fig. 5. For the Bragg scatter i the new value of the angle $\phi(i)$ is

$$\phi(i) = \phi(i-1) + \omega t_{slot}(i) \tag{12}$$

where ω is the Larmor precession frequency. Therefore, for this Bragg scatter we have $\delta_{so}(i) = \cos[\phi(i)] \times 3.27 \times 10^{-4}$ radians.

For all 136 reflections we have for each j^{th} trajectory

$$\delta^{136}_{so(j)} = \sum_{i=1}^{136} \delta_{so}(i) = \sum_{i=1}^{136} \cos[\phi(i)] \times 3.27 \times 10^{-4} \tag{13}$$

and

$$\delta^{136}_{so(tot)} = \sum_{j=1}^{11} \delta^{136}_{so(j)} \tag{14}$$

for all 11 trajectories.

From Eq. 14, we expect to have a Schwinger spin-orbit rotation compared to an ideal crystal that is

$$S = \frac{\delta^{136}_{so(tot)}}{11 \times 0.0473} \tag{15}$$

At the optimum setting for B_z for this crystal the normalized amplitude is S=0.76. Based on uncertainties in the slot width and considering beam non-uniformity and divergence, we estimate the accuracy in the simulated amplitude to be ≤ 1 %. In addition we were able to use different values of the initial ϕ_0 at the first reflection by setting the position of the rotator coil to be at different distances D_r from the first reflection. These predictions from the simulation were then compared to measurements of S for different settings of B_z and ϕ_0.

IV. MEASUREMENTS AND SYSTEMATIC UNCERTAINTIES

A. Data collection

The established pattern for data collection in the reflected beam was to map out the Schwinger signal P_z^{tot} at eight selected distances between the spin rotator coil and the first reflection on the silicon crystal, covering the full 20.0 mm described above. Because the count rates at each location were very modest it was decided to collect these data in 5 or more full passes of the eight rotator locations and then add together the data when the 5 passes had completed. The entire process, including precisely translating the rotator coil, starting and stopping data collection and storage, and also recording the monitoring data, was fully automated and took nearly 5 days to complete the data collection for one setting of B_z. This process was performed for different values of B_z around the initial value of B_z^0. In addition, repeated measurements at identical settings were taken for several values of B_z to test the reproducibility of our measurements.

B. Data analysis

In a typical polarization analysis experiment [20], one would measure the count rates for opposite spin polarizations and compute the asymmetry in the count rate, $(N_+ - N_-)/(N_+ + N_-)$, where N_+ and N_- correspond to spin up and spin down, respectively. These spin orientations could be established using the upstream precession coil π-flipper described in Sec III E 1. Instead the experiment was conducted as described in Secs. III E 2 and

III F by changing the distance between the rotator coil and the first Bragg reflection, D_r, which changes the spin orientation, ϕ_0, on the first reflection. Hence by varying distances D_r over the full 20 mm spatial Larmor period we were able to measure the effect of the spin-orbit interaction over a 2π range of ϕ_0 values. The resulting count rates for the reflected beam as a function of D_r yielded a sinusoidal oscillation around the average count rate, which we refer to as the Schwinger oscillation. The average count rate was the observed count rate for the rotator locations that position the neutron spin along the x-axis ($\phi_0 = \pi/2,\ 3\pi/2$), for which the spin-orbit interaction is zero.

Empirically, for each value of D_r we computed $\Delta(D_\mathrm{r})$, which is the deviation from the mean number of reflected counts

$$\Delta(D_\mathrm{r}) = \frac{[R(D_\mathrm{r}) - B_0]/M(D_\mathrm{r}) - (R_0 - B_0)/M_0}{(R_0 - B_0)/M_0}, \quad (16)$$

where $R(D_\mathrm{r})$ and $M(D_\mathrm{r})$ are the number of counts in the reflected and direct beam detectors for a given rotator location, respectively, B_0 is the number of background counts (see Sec. III), and R_0 and M_0 are the mean number of counts in the reflected and direct beam detectors averaged over all rotator locations, respectively. The uncertainties in each $\Delta(D_\mathrm{r})$ are also calculated.

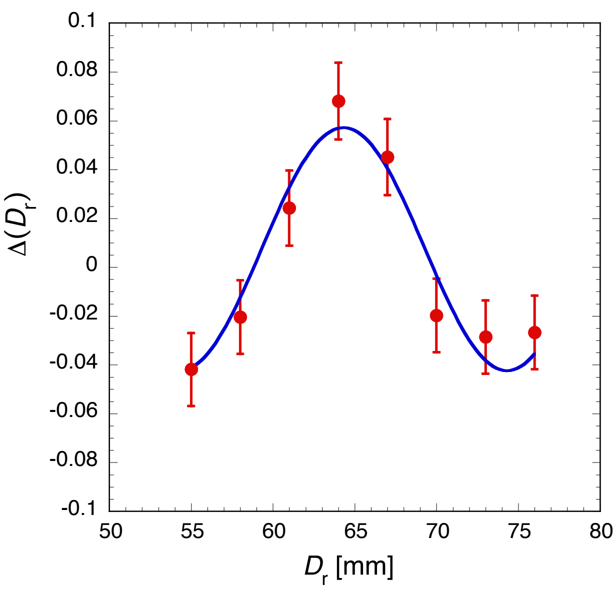

FIG. 6: Typical data obtained from the reflected beam by translating the rotator coil, shown as solid red circles. $\Delta(D_\mathrm{r})$ is defined in Eq. (16). The magnetic field was B_z^0=1.7672 mT (17.672 G). The error bars indicate the standard uncertainty due to counting statistics only. The solid blue line shows a fit to Eq. (17).

Fig. 6 shows typical data obtained by translating the rotator coil. For a typical 6000 s period, $R_0 \approx 1000$, $B_0 \approx 120$, and $M_0 \approx 3.1 \times 10^6$. The $\Delta(D_\mathrm{r})$ values for 8 such periods were averaged to obtain the data shown. As the rotator position is scanned through the spatial Larmor period, the neutron spin direction incident on the crystal is rotated in the x-y plane. The data are then fitted to

$$\Delta(D_\mathrm{r}) = O + S N_\mathrm{R} \delta'_\mathrm{so} \sin[2\pi(D_\mathrm{r} - z_0)/\Lambda] \quad (17)$$

The expected amplitude of the Schwinger oscillation for a perfect crystal slot with the optimum B_z for a spin precession of π rad on each crossing of the slot would be S=1 and $N_\mathrm{R}\delta'_\mathrm{so} = 136\delta'_\mathrm{so}$. For our measurements $136\ \delta'_\mathrm{so} = 136\ \delta_\mathrm{so} P_\mathrm{p} A_a$, where $P_\mathrm{p} A_a = 14/16$ for the measured instrumental flipping ratio of 15 and $136\ \delta_\mathrm{so}$= 0.0473 rad is the total Schwinger rotation after 136 Bragg reflections in a perfect slotted silicon crystal. In Eq. 17 O, S and z_0 are free parameters in the fit to measured data. For our (geometrically imperfect crystal, S is expected to be 0.76. The offset parameter O allows for any difference between the value of $(R_0 - B_0)/M_0$ employed and the value that yields the best fit to a sinusoid. The parameter $z_0(2\pi/\Lambda)$ is a phase factor, where z_0 is in units of millimeters and 2π of actual phase corresponds to the spatial Larmor period of Λ = 20.0 mm. At a magnetic field B_z^0, O and z_0 are expected to be near zero. For the data shown in Fig. 6, $O = 0.0074 \pm 0.0055$, $S = 1.20 \pm 0.18$, and $z_0 = (-0.31 \pm 0.52)$ mm, where the uncertainties are determined from the fit.

To see if the sense of the observed change in the count rate is consistent with what we expect given the applied magnetic fields we look in detail at the interaction of the neutron MDM (which points opposite to the neutron spin vector) with the various relevant magnetic fields as the neutron transits from the polarizer to the analyzer and detector. The magnetic field points down ($-\hat{x}$ direction) in the polarizer, rotator and analyzer and it is pointed upstream ($-\hat{z}$ direction) in the four-coil system. The supermirror polarizer transmits a neutron with its MDM pointed down ($-\hat{x}$ direction), which rotates to be pointed upstream ($-\hat{z}$ direction) in the four-coil system. The resultant field in the rotator coil, B_net, is pointed downward at $\approx 45°$ angle with components in the $-\hat{x}$ and $-\hat{z}$ directions, so that the torque $\vec{\mu}_\mathrm{n} \times \vec{B}_\mathrm{net}$ on the MDM is in the $\hat{y}$ direction and thus the MDM rotates to be pointed down ($-\hat{x}$ direction). Past the rotator the field is again upstream ($-\hat{z}$ direction) and the torque on the MDM is in the $-\hat{y}$ direction implying that the MDM will rotate counterclockwise about the $-\hat{z}$ direction. For D_r= 55 mm, the MDM rotates by 2.75×2π to be pointed along the $+\hat{y}$ direction at the first reflection, as seen in Fig. 1. The spin-orbit interaction is proportional to $\vec{v} \times \vec{E}$, where the relevant component of the neutron velocity, $\vec{v}$, is along the $+\hat{y}$ direction and the electric field $\vec{E}$ is along the $-\hat{z}$ direction at the first reflection, hence from Eq. (1) the induced effective magnetic field $\vec{B}_\mathrm{eff}$ is pointed down ($-\hat{x}$ direction) and the torque on the MDM is downstream

($\hat{z}$ direction). This torque rotates the MDM towards the $\hat{z}$ direction, ie opposite to the magnetic field in the four-coil system. Upon entering the analyzer, this $\hat{z}$ component adiabatically rotates to become an $\hat{x}$ component. Since the analyzing supermirror transmits neutrons with MDM along $-\hat{x}$ (as for the polarizer), the count rate decreases, in agreement with our observations.

C. Magnetic field dependence

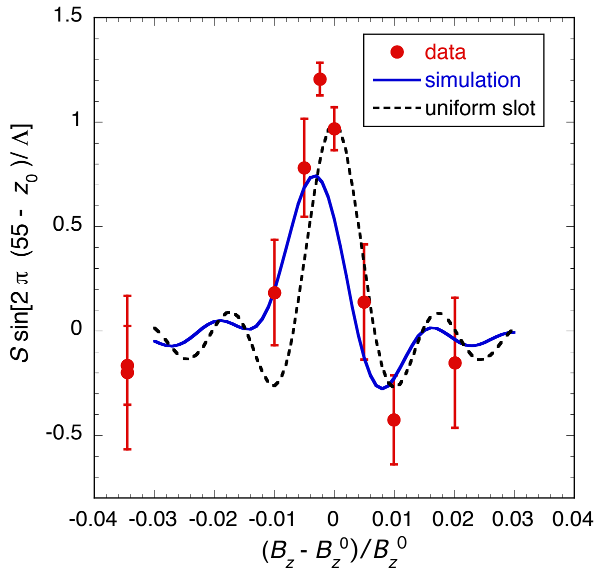

FIG. 7: The value of the fitted function $S\sin[2\pi(D_{\rm r}-z_0)/\Lambda]$ determined from the fitted values of S and z_0 and evaluated at $D_{\rm r}$ = 55 mm for each B_z. The central magnetic field is B_z^0 = 1.7672 mT (17.672 G). The data are shown by solid red circles and the simulation for our crystal slot is shown by the solid blue line. The error bars represent the combined standard uncertainty determined from the uncertainties in the fit parameters S and z_0. In addition, the simulation for a slot with uniform width is shown as a black, dashed line.

It was noted in Sec. III E 2 that this method of using repeated Bragg scatters down the crystal slot for studying the Schwinger spin-orbit effect depends sensitively on matching the four-coil axial magnetic field to the Larmor precession of the neutron crossing the slot. To study this dependence, data such as shown in Fig. 6 were taken at eight different values of the magnetic field B_z varied around B_z^0=1.7672 mT (17.672 G). The fit of Eq. 17 to each of these data at different B_z yielded $\Delta(D_{\rm r})$ each with its amplitude S and phase z_0. In Fig. 7 we have plotted the value of $S\sin[2\pi(D_{\rm r}-z_0)/\Lambda]$ determined from the fitted values of S and z_0 and evaluated at $D_{\rm r}$ = 55 mm for each B_z. We also show the predicted value simulated as described in Sec. III F. For comparison, this same simulation was done for the case of a crystal with a uniform slot with a width matched to the magnetic field B_z^0. As seen in Fig. 7 for this uniform slot $S\sin[2\pi(D_{\rm r}-z_0)/\Lambda]$ is unity at B_z^0 and is symmetric about B_z^0. This plot shows convincingly that to find the Schwinger signal one must set B_z to have the correct Larmor precession frequency to within 1 %.

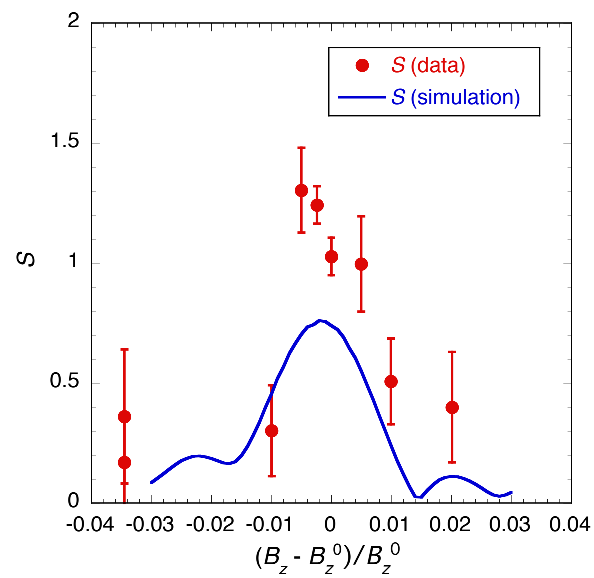

FIG. 8: The variation of S from the fit of Eq. 17 to data collected in the reflected beam at different values of B_z. The central magnetic field is B_z^0 = 1.7672 mT (17.672 G). The data are shown by solid red circles and the simulation is shown by the solid blue line. The error bars represent the standard uncertainties in the fit parameter S.

Fig. 7 shows the amplitudes S at $D_{\rm r}$=55 mm, which were determined from the fits shown in Fig. 6. In Figs. 8 and 9 we show the both the data and the simulation for the individual amplitude and phase parameters. Fig. 8 shows the measured dependence of S on the magnetic field B_z produced by the four-coil assembly. Comparing the measured values to the predictions in Figs. 7 and 8 shows qualitatively good agreement. However, quantitatively the measured values, especially near the signal maximum, are systematically larger than predicted. As the magnetic field is varied around B_z^0, the resulting phase of the Schwinger oscillation changes as shown in Fig. 9. The phase data follow the curve obtained using the simulation, but are generally more positive. However, we estimate a fixed, systematic uncertainty of 1 mm in all values of $D_{\rm r}$ (not shown in Fig. 9), associated with the uncertainty in the orientation of the MDM at the first reflection from the crystal.

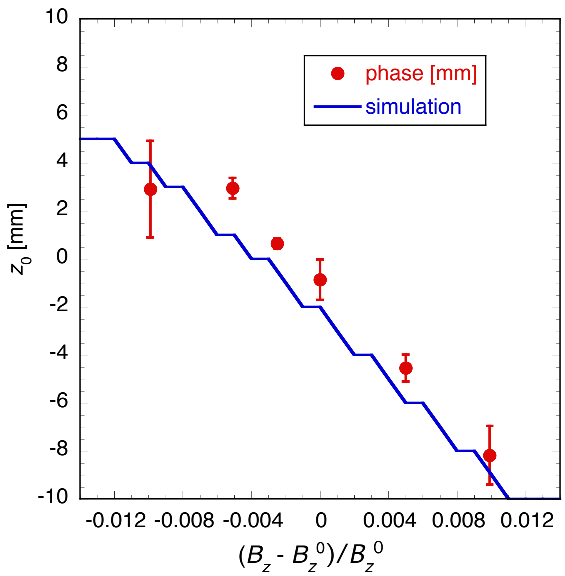

FIG. 9: The variation of z_0 from the fit of Eq. 17 to data collected in the reflected beam at different B_z. The central magnetic field is $B_z^0 = 1.7672$ mT (17.672 G). The values of z_0 extracted from the data are shown as red solid circles and the calculation is shown as a solid blue line. The error bars represent the standard uncertainties in the fit parameter z_0.

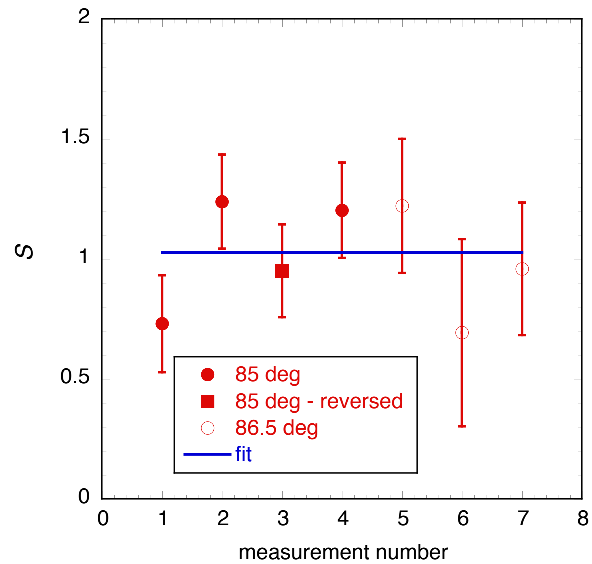

FIG. 10: A series of measurements of the Schwinger oscillation (magnetic field was 1.7672 mT (17.672 G)). Data obtained at $\theta_{\rm B} = 85°$ are shown by red filled circles, at $\theta_{\rm B} = 85°$ with the rotator coil current reversed by a red filled square, and at $\theta_{\rm B} = 86.5°$ by red open circles. The error bars shown represent the fit uncertainties for each measured Schwinger oscillation. The red line shows a fit of the seven points to a flat line, yielding $S = 1.027 \pm 0.078$ with a reduced $\chi^2 = 1.1$. See the text for further discussion.

D. Systematic tests and uncertainties

1. *Systematic tests*

As discussed in Sec. II, the value of $P_z^{\rm tot}$ is independent of Bragg angle. We performed measurements at Bragg angles of 86.5° (194 reflections) and 85° (136 reflections) and observed that the amplitude of the Schwinger spin-orbit rotation for 86.5° was consistent with that measured at 85° (see Fig. 10).

Figs. 10 and 11 show the results of repeated measurements obtained at $B_z^0 = 1.7672$ mT (17.672 G) and $0.9975 B_z^0$ over a period of several months. In Fig. 10 one data point was obtained with the rotator coil current reversed. In this case we expect the oscillation in the asymmetry to invert and indeed we found $z_0 = (10.2 \pm 0.6)$ mm for this datum, which corresponds to $\Lambda/2$ within uncertainties.

2. *Spin transport oscillation*

The primary systematic error is associated with the upstream spin alignment. As described in Sec III E 1, the neutrons transitioning from the upstream permanent magnet guide fields are presumed to adiabatically align with the magnetic field in the four-coil system, B_z and then travel to the rotator coil. If this adiabatic transition is not complete, a residual component of the neutron spin will be transverse to B_z. The result will be a component along the z-direction after the neutron passes through the rotator coil and this will be added to the Schwinger spin-orbit induced z-component. To study this we carried out a series of measurements in the direct beam by moving the analyzer into the direct beam. We observed a small oscillation in the analyzer count rate as the rotator coil was moved. As shown in Fig. 12 the oscillation had a periodic length of 20.0 mm, consistent with what would be expected from a Larmor precession in the 1.7672 mT (17.672 G) four-coil magnetic field. We refer to this as the spin transport oscillation (STO). We found that the amplitude of the STO was sensitive to physical adjustment of the guide field arrangement. We could not completely eliminate the STO, hence we tried replacing the guide field arrangement with a longitudinal coil to simplify and potentially improve the spin transport from the supermirror polarizer to the four-coil magnetic field. However, even after adjusting the current in this coil the minimum amplitude of the STO was unchanged. It corresponded to the neutron spin at an angle of 0.0096 rad, hence the spin transport efficiency was $\cos(0.0096) = 0.99995$. If we assume that the STO is preserved in the reflected beam, it would yield, in the absence of any Schwinger oscillation, an oscillation with an amplitude $S = 0.24$ but an unknown phase. This systematic effect would combine with the Schwinger oscillation. Most simply considered,

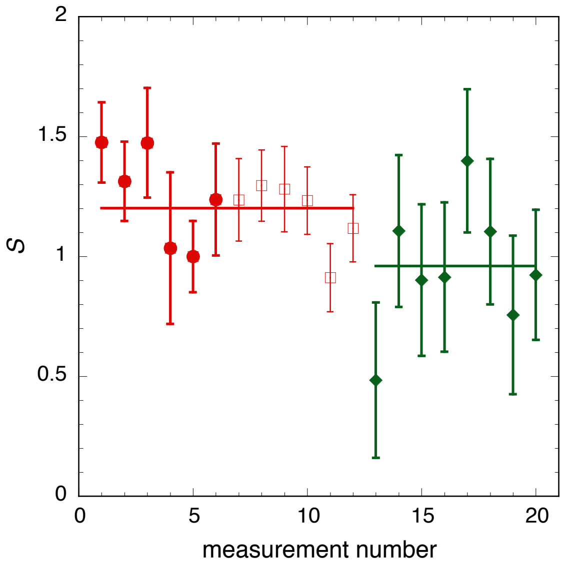

FIG. 11: A series of measurements of the Schwinger oscillation (magnetic field was 0.9975*1.7672 mT (0.9975*17.672 G)). Data were obtained with the permanent magnet guide field (red solid circles), the longitudinal coil with currents between 2.0 and 3.0 A (red open squares), and with polarized ^{3}He neutron spin filters (green diamonds)(see Sec. IV D 3). (The relevant averages of the first six data points, which were obtained with the permanent magnet guide field, correspond to the data points shown in Fig. 7, 8, and 9.) The error bars shown represent the standard uncertainties in the fitted amplitudes for each measured Schwinger oscillation. The red line shows a fit of the 12 points obtained with supermirrors to a flat line, yielding $S = 1.201 \pm 0.048$ with a reduced $\chi^2 = 1.1$. The green line shows a fit of the 8 points obtained with neutron spin filters, yielding $S = 0.960 \pm 0.109$ with a reduced $\chi^2 = 0.7$. See the text for further discussion.

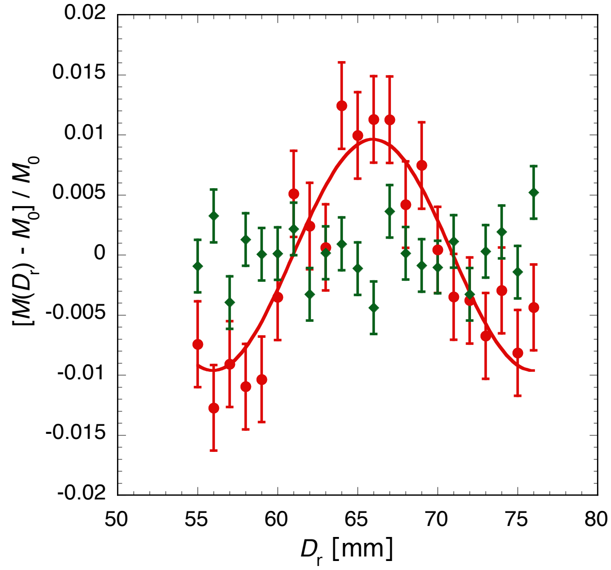

FIG. 12: Plots of the fractional deviation from the mean count rate with an analyzer in the direct beam. The red solid circles show the typical spin transport oscillation (STO) using supermirrors, obtained with a current of 2.5 A in the longitudinal coil. The red line shows a fit to a sinusoid that has an amplitude of 0.0096 ± 0.0010. In contrast, the green solid diamonds show the absence of this systematic effect when polarized ^{3}He-based spin filters were employed to polarize and analyze the neutron beam; in this case the fit (not shown) yields an amplitude consistent with zero (-0.0006 ± 0.0006). The error bars represent the standard uncertainty due only to counting statistics.

the two worst case scenarios would be direct addition (in phase) or subtraction (opposite phase) of the Schwinger oscillation and the STO, which would have the maximum effect on the fitted amplitude but no effect on the phase. If the STO and the spin-orbit oscillation have any other relative phase, a smaller net amplitude in the reflected beam would occur and the phase of this net oscillation would be affected.

The effects of this issue were studied by varying the current in the longitudinal coil. See Fig. 12 for a typical STO that was obtained with a current of 2.5 A. For a range of currents between 2 A and 3 A we found that the amplitudes of STOs were similar. However, the phases were different, which would be expected to affect the fitted amplitude of the reflected beam oscillation differently. Still, the effect on the fitted amplitude of the reflected beam oscillation at different currents in this range was observed to be within the fitted uncertainties (see Fig. 11).

We also decreased the current so as to degrade the spin transport and thereby increased the amplitude of the STO to a value that would correspond to $S = 0.9$ if it were observed in the reflected beam in the absence of a spin-orbit effect. The changes in the amplitudes observed in the reflected beam were consistent with what would be expected from the larger STO amplitudes, and phase shifts were also observed. We have assigned a systematic uncertainty in S of 0.18 due to the uncertainty in the effect of the STO. This value was obtained from the standard deviation in the range of fitted amplitudes that results when a simulated STO with an amplitude of 0.24 and a range of phases were added to a simulated Schwinger oscillation.

In Fig. 11 the first six measurements were obtained with the permanent magnet guide field arrangement and the last six were obtained using the longitudinal coil at six currents of between 2.0 A and 3.0 A. For the latter, we found the STO amplitudes to be similar but with different phases. The reduced χ^2 is 1.1.

3. *Measurements with polarized ^{3}He spin filters*

The persistent issue with spin transport motivated us to employ nuclear-spin polarized ^{3}He-based neutron spin filters (NSFs) [19, 21] to polarize and analyze the neutron beam. These devices rely on the strong spin dependence of the absorption of neutrons by ^{3}He to transmit primarily one spin state. We employed spin-exchange optical pumping (SEOP), in which electronic polarization is produced in a Rb/K vapor by optical pumping with high power diode lasers and and transferred to the ^{3}He nuclei via spin-exchange collisions.

Since it was not practical to perform SEOP continuously in this apparatus, cells were polarized externally and then transported to the apparatus. One cell was located in the incident beam immediately upstream of the spin rotator and the other cell in the reflected beam just downstream of the end of the slotted crystal. Because the cells selected neutron spin along the four-coil magnetic field axis B_z, no spin rotations were required. The absence of spin rotations avoided the issues with imperfect spin transport in the supermirror scheme. The supermirrors were translated out of the neutron beam. Fig. 12 shows that there was no discernable STO using spin filters. We found it was necessary to replace both the polarizer and the analyzer supermirrors with neutron spin filters to eliminate the STO.

The cells had intrinsic relaxation times for spin polarization of the ^{3}He gas of between 400 h and 520 h, which were not substantially compromised by magnetic field gradients due to the high homogeneity of our four-coil magnetic field. Some gradient-induced relaxation was observed for the polarizer cells, which were required to be further from the field center because of the rotator. The typical relaxation times observed in actual operation were between 370 h and 520 h for analyzer cells and 310 h for the polarizer cells. Typical initial ^{3}He polarization values were between 76 % and 84 %. Despite these excellent values for both ^{3}He polarization and relaxation times, the initial overall transmission was still roughly a factor of two below that of the supermirror approach, and it declined by another factor of three during the course of a 5-day run cycle. Hence we focused on obtaining sufficient data with the ^{3}He cells at $B_z = 0.9975B_z^0$ for comparison with the results obtained with the supermirror polarizer and analyzer.

Due to the time dependence of the ^{3}He polarization, data acquired for 6000 s at each rotator location were corrected for the declining overall transmission and flipping ratio. The initial and final ^{3}He polarizations and thus the relaxation times were determined by neutron transmission measurements on each cell at the start and end of the typical 5 day run cycles. From these data the overall time-dependent transmission and flipping ratio were determined. The typical initial and final flipping ratios were ≈ 17 and ≈ 6, respectively. We directly monitored the decay of the polarizer transmission by tracking the direct beam count rate. The decay of the analyzer transmission was also monitored via the ratio of the reflected beam count rate to the direct beam count rate. The background rate was higher than that obtained with the supermirrors due to shielding of the detector by the analyzing supermirror and its yoke. To reduce the background, an array of polyethylene blocks was employed to surround the neutron beam near the detector, yielding a typical rate of $B_0^{\mathrm{NSF}}= 175$ counts in a 6000 s run, about 1.5 times higher than that obtained with the supermirrors. The combined uncertainty in S from the determination of background, ^{3}He polarization, and ^{3}He relaxation time were negligible compared to the uncertainty in the fit to Eq. 17.

NSFs were employed for six run cycles at a magnetic field 0.9975*1.7672 mT (0.9975*17.672 G) . The fits to Eq. 17 yielded $S = 0.960 \pm 0.109$ with a reduced χ^2 of 0.74 (see Fig. 11), consistent with the value of 1.201 $\pm$ 0.048 (statistical) $\pm$ 0.18 (systematic) obtained with supermirrors.

V. CONCLUSION

We have successfully demonstrated the technique of measuring the Schwinger spin-orbit induced polarization rotation in multiple Bragg reflections to study the neutron spin-orbit interaction. The dependence of both the amplitude and phase of the Schwinger oscillation observed by translating the spin rotator are consistent with predictions.

Data obtained with supermirrors to polarize and analyze the neutron beam were affected by a systematic effect associated with spin transport. An uncertainty was assigned for this systematic by measurements in the direct beam and also by varying the spin transport. In addition, the effect was completely eliminated using neutron spin filters and the results in this configuration were consistent within uncertainties with the supermirror-based results. The total uncertainty for the supermirror-based result is dominated by the systematic uncertainty whereas the total uncertainty for the spin filter based result is dominated by statistical uncertainty.

Our results for the magnitude of the induced Schwinger oscillation measured by the parameter S are a factor of 1.26 (spin filters) to 1.58 (supermirrors) larger than was calculated in Sec. II based on the description of the spin-orbit interaction in Refs. [1, 8]. The origin of this discrepancy is unknown. In the context of the existing theory, our results would indicate that the electric field sensed by the neutron in its passage through multiple Bragg reflection is higher than that given by the screening factor. Experimental values and Hartree-Fock and density functional theory calculations of the atomic screening factor for the silicon 220 reflection agree within better than 1 % [17, 22, 23]. However, these calculations do not consider crystal imperfections and impurities. The results of Finkelstein [10] indicated a factor of 1.18 larger spin-orbit effect in silicon than expected; our results show the same trend but to a larger degree.

An improved experiment would require an efficient apparatus for longitudinal polarization and a slotted crystal with higher reflectivity and a uniform slot. The former could be accomplished with continuously operating neutron spin filters.

ACKNOWLEDGEMENTS

We thank Wangchun Chen for providing some of the excellent ^{3}He cells and the longitudinal coil employed, and for useful discussions; Valparaiso University students Tim Olson, Ansel Hilmer, Benjamin Barber, and Samuel Brandt; Fred Wietfeldt for useful discussions; and early experimental contributions by Helmut Kaiser. The NIST effort was partially supported by the U.S. Dept. of Energy, Office of Nuclear Physics, under Interagency Agreement 89243019SSC000025. D.D.K. is grateful for support from the Julian Schwinger Foundation and the NIST Summer Undergraduate Research Fellowship program.

[1] J. Schwinger, Phys. Rev. **73**, 407 (1948).
[2] R.G.P. Voss and R. Wilson, Phil. Mag. **8**, 175 (1956).
[3] J.T. Sample, Can. J. Phys. **34**, 36 (1956).
[4] Iu. A. Aleksandrov and I.I. Bondarenko, Soviet Physics JETP **4**, 612 (1957).
[5] Iu. A. Aleksandrov, Soviet Physics JETP **6**, 228 (1958).
[6] V.M. Koprov, Soviet Physics JETP **11**, 459 (1960).
[7] S.B. Gerasimov, A.I. Lebedev and V.A. Petrunkin, Soviet Physics JETP **16**, 1321 (1963).
[8] C.G. Shull. Phys. Rev. Lett. **10**, 297 (1963).
[9] G.P. Felcher and S.W. Peterson, Acta Cryst. A **31**, 76 (1975).
[10] K. Finkelstein. Ph. D. Thesis (Mass. Inst. of Tech., 1987).
[11] C.G. Shull and R. Nathans, Phys. Rev. Lett. **19**, 384 (1967).
[12] S.K. Lamoreaux and R. Golub, J. Phys. **G36**, 104002 (2009).
[13] C.A. Baker *et al.*, Phys. Rev. Lett. **97**, 131801 (2006).
[14] V.V. Fedorov and V.V. Voronin, J. Phys. Soc. Japan Conf. Proc. **22**, 011007 (2018).
[15] V.V. Fedorov, I.A. Kuznetsov, E.G. Lapin, S.Yu. Semenikhin, and V.V. Voronin, Nucl. Instrum. Meth. Phys. Res. B **252**, 131 (2006).
[16] V.F. Sears, Phys. Rep. **141**, 281 (1986).
[17] J.M. Zuo, P. Blaha, and K. Schwarz, J. Phys.: Condens. Matter **9**, 7541 (1997).
[18] A. Ioffe, D.L. Jacobson, M. Arif, M. Vrana, S. A. Werner, P. Fischer, G. L. Greene, and F. Mezei, Phys. Rev. A **58**, 1475 (1998).
[19] T.R. Gentile, P.J. Nacher, B. Saam, and T.G. Walker, Rev. Mod. Phys. **89**, 045004 (2017).
[20] W. Gavin Williams, Polarized Neutrons, (Oxford, New York, 1988).
[21] W.C. Chen, T.R. Gentile, C.B. Fu, S. Watson, G.L. Jones, J.W. McIver, and D.R. Rich, Journal of Physics: Conf. Series **294**, 012003 (2011).
[22] M. Deutsch, Phys. Rev. B **45**, 646 (1992).
[23] J. Pere, M. Gelize-Duvignau and A. Lichanot, J. Phys.: Condens. Matter **11**, 5827 (1999).